Triclosan impairs excitation–contraction coupling and Ca^{2+} dynamics in striated muscle

Gennady Cherednichenko[a,1], Rui Zhang[a,1], Roger A. Bannister[b,1], Valeriy Timofeyev[c], Ning Li[c], Erika B. Fritsch[a], Wei Feng[a], Genaro C. Barrientos[a], Nils H. Schebb[d], Bruce D. Hammock[d,2], Kurt G. Beam[e], Nipavan Chiamvimonvat[c,f], and Isaac N. Pessah[a,2]

[a]Department of Molecular Biosciences, School of Veterinary Medicine, [c]Division of Cardiovascular Medicine, Department of Internal Medicine, and [d]Department of Entomology and Cancer Center, University of California, Davis, CA 95616; [b]Cardiology Division, Department of Medicine, and [e]Department of Physiology and Biophysics, University of Colorado Denver-Anschutz Medical Campus, Aurora, CO 80045; and [f]Department of Veterans Affairs, Northern California Health Care System, Mather, CA 95655

Contributed by Bruce D. Hammock, July 13, 2012 (sent for review June 18, 2012)

Triclosan (TCS), a high-production-volume chemical used as a bactericide in personal care products, is a priority pollutant of growing concern to human and environmental health. TCS is capable of altering the activity of type 1 ryanodine receptor (RyR1), but its potential to influence physiological excitation–contraction coupling (ECC) and muscle function has not been investigated. Here, we report that TCS impairs ECC of both cardiac and skeletal muscle in vitro and in vivo. TCS acutely depresses hemodynamics and grip strength in mice at doses ≥12.5 mg/kg i.p., and a concentration ≥0.52 μM in water compromises swimming performance in larval fathead minnow. In isolated ventricular cardiomyocytes, skeletal myotubes, and adult flexor digitorum brevis fibers TCS depresses electrically evoked ECC within ∼10–20 min. In myotubes, nanomolar to low micromolar TCS initially potentiates electrically evoked Ca^{2+} transients followed by complete failure of ECC, independent of Ca^{2+} store depletion or block of RyR1 channels. TCS also completely blocks excitation-coupled Ca^{2+} entry. Voltage clamp experiments showed that TCS partially inhibits L-type Ca^{2+} currents of cardiac and skeletal muscle, and [^{3}H]PN200 binding to skeletal membranes is noncompetitively inhibited by TCS in the same concentration range that enhances [^{3}H]ryanodine binding. TCS potently impairs orthograde and retrograde signaling between L-type Ca^{2+} and RyR channels in skeletal muscle, and L-type Ca^{2+} entry in cardiac muscle, revealing a mechanism by which TCS weakens cardiac and skeletal muscle contractility in a manner that may negatively impact muscle health, especially in susceptible populations.

cachexia | calcium regulation | heart failure | muscle contraction | L-type current

Triclosan [5-chloro-2-(2,4-dichlorophenoxy)phenol; TCS] is a bactericide found in many personal care products and has been incorporated into cleaning supplies, bedding, clothes, fabrics, shoes, carpets, plastics, and medical devices (1–3). Introduced over 40 y ago, TCS production has dramatically increased over the past two decades, exceeding 1 million pounds produced annually when assessed in 1998 by the US Environmental Protection Agency (USEPA) (1). Based on the available data, TCS is well tolerated following oral or dermal exposure, and several aspects of safety have been assessed in animal models (2). However, TCS has been detected in raw and treated waste water, natural streams, sewage sludge, fish, and human samples of urine, plasma, and breast milk (4–9), raising concerns of its potential long-term adverse impacts on environmentally sensitive species and human health. There is emerging evidence that TCS can disrupt endocrine signaling and immune function, inhibit carboxylesterase activity, bioaccumulate in organisms, and cause bacterial resistance (10–15).

Structurally TCS, a polychlorinated diphenyl ether, shares chemical properties with nondioxin-like persistent organic pollutants, such as the hydroxylated metabolites of *ortho*-substituted polychlorinated biphenyls (PCBs) and polybrominated diphenyl ethers (PBDEs). Receptor-based screens (12, 16) revealed that similar to PCBs (17) and PBDEs (18), TCS has potential for direct interaction with type 1 and type 2 ryanodine receptors (RyR1 and RyR2), supporting a possible convergent mechanism of action among structurally related noncoplanar halogenated persistent organic pollutants. Despite extensive analysis of TCS efficacy and toxicity, the potential of TCS to alter cardiac and skeletal muscle physiology have not been previously reported (2). Considering that RyRs are intracellular channels that mediate the release of Ca^{2+} from the sarcoplasmic reticulum (SR), necessary for excitation–contraction coupling (ECC) in skeletal and cardiac muscle, alteration in ECC by TCS may promote acute or long-term impacts on muscle health in human populations and environmentally sensitive species. Moreover, mutations in the *RYR1* gene are linked to dysregulated Ca^{2+} homeostasis in heritable diseases of skeletal muscle, including malignant hyperthermia and central core disease (19, 20), and aging related muscle weakness (21). Mutations in the *RYR2* gene are responsible for arrhythmogenic disorders, including catecholaminergic polymorphic ventricular tachycardia and arrhythmogenic right ventricular dysplasia type 2 (20, 22), and are etiological contributors to ischemic heart failure (23). Considering the critical role of RyR channels in muscle physiology and pathophysiology, we deemed it necessary to investigate whether TCS has the potential of impairing ECC of cardiac and skeletal muscle in vivo and in vitro to better assess the potential risks associated with its pervasive use.

Results

TCS Depresses Cardiac Hemodynamics and Skeletal Muscle Contractility in Vivo. Whether acute exposures to TCS were capable of altering functional parameters of striated muscle were investigated using three in vivo tests. First, anesthetized mice instrumented with a pressure-sensitive catheter were exposed to a single intraperitoneal dose of TCS (6.25, 12.5, or 25 mg/kg) or an equal volume of vehicle (20% vol/vol DMSO in saline, 200 μL). In contrast to vehicle control, mice receiving TCS showed significantly impaired hemodynamic functions within 10 min of exposure in a dose-dependent manner. Cardiovascular impairments included significantly reduced cardiac output, lower left ventricular end-diastolic volume, and reduction in the maximum time-derivative of the left ventricular pressure development (Fig. 1*A*). Of note, the highest-dose group (25 mg/kg) exhibited a 25.3 ± 15.7% decrease in

Author contributions: G.C., R.Z., R.A.B., V.T., N.L., E.B.F., W.F., G.C.B., N.H.S., B.D.H., K.G.B., N.C., and I.N.P. designed research; G.C., R.Z., R.A.B., V.T., N.L., E.B.F., W.F., G.C.B., and N.H.S. performed research; N.H.S. and B.D.H. contributed new reagents/analytic tools; G.C., R.Z., R.A.B., V.T., N.L., E.B.F., W.F., G.C.B., N.H.S., B.D.H., K.G.B., N.C., and I.N.P. analyzed data; and G.C., R.Z., R.A.B., E.B.F., N.H.S., B.D.H., K.G.B., N.C., and I.N.P. wrote the paper.

The authors declare no conflict of interest.

[1]G.C., R.Z., and R.A.B. contributed equally to this work.

[2]To whom correspondence may be addressed. E-mail: bdhammock@ucdavis.edu or inpessah@ucdavis.edu.

This article contains supporting information online at www.pnas.org/lookup/suppl/doi:10.1073/pnas.1211314109/-/DCSupplemental.

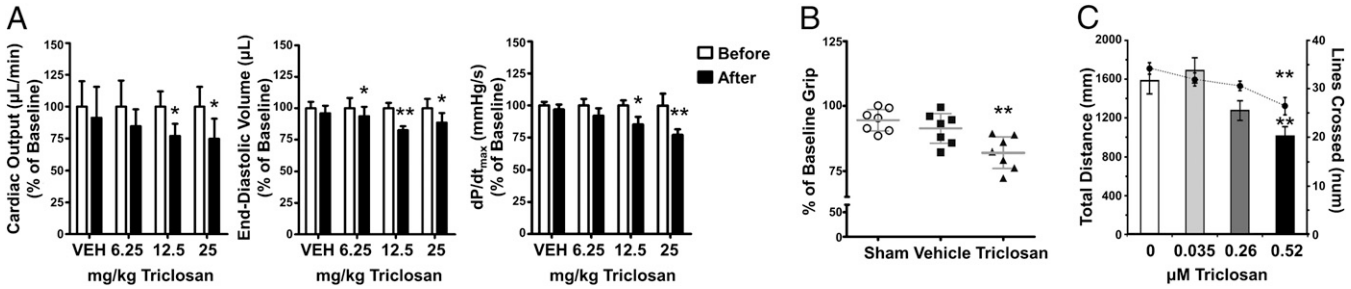

Fig. 1. TCS depresses hemodynamics and in vivo skeletal muscle function. (*A*) Mice (vehicle: $n = 3$; TCS: $n = 4$–5) were anesthetized with ketamine/xylazine and instrumented with recording PV catheter advanced into the left ventricle via the carotid artery. After dosing with TCS (20% DMSO vol/vol in 200 μL) intraperitoneally, both 12.5 and 25 mg/kg groups experienced significant reductions in cardiac output, ventricular filling, and left ventricular developed pressure. Error bars represent SEM. $*P < 0.05$; $**P < 0.01$, one-tailed paired *t* test. (*B*) Grip strength was assessed in mice ($n = 7$ per group) before and after sham, vehicle (30 μL DMSO), or 40 mg/kg TCS intraperitoneal injection. Postdose grip was significantly lower in the TCS group compared with both sham and vehicle. Gray bars represent mean and 95% CI. $**P < 0.01$, ANOVA. (*C*) Larval fathead minnow ($n = 36$ per concentration) were exposed up to 7 d to vehicle (0.01% MeOH), or TCS (0.035, 0.26, or 0.52 μM). Swimming behavior was assessed by nonprovoked (distance traveled, bar graph) and forced (lines crossed in 60 s, line graph) activity. A decreasing trend was seen for both swimming parameters, with significance found in the 0.52-μM group. Error bars represent SEM. $**P < 0.01$, Kruskal-Wallis.

cardiac output, implying that TCS was capable of eliciting severe cardiovascular impairments. The administration of TCS to mice led to dose-dependent plasma levels of unconjugated TCS, with up to 0.31 ± 0.09 μM detected in the samples from the 25-mg/kg dose group (Fig. S1).

Second, skeletal muscle function was assessed using a grip-strength meter by measuring the total force produced by the limbs of mice at test times up to 60 min after a single 40 mg/kg i.p. TCS dose. Normalized to predose baseline, TCS-treated animals had a mean decrease of 18% [95% confidence interval (CI): 12.0–24.0%] in grip strength, which was significantly lower than both sham- and vehicle-injected groups (Fig. 1*B*). No statistical difference was seen between sham- and vehicle-injected groups. These impairments were transitory and exposed mice recovered grip strength comparable to baseline 24 h after dosing.

Third, the fathead minnow (*Pimephales promelas*) has been extensively used as model organism to study the potential impacts of aquatic pollutants on teleost (24). Considering the pervasive nature of TCS in the aquatic environment, and TCS-mediated impairments detected in mammalian striated muscle, we investigated whether TCS adversely affected fish swimming performance. Larval fathead minnow were exposed to TCS (0.035, 0.26, or 0.52 μM) for up to 7 d and swimming performance assessed at test termination. At the highest TCS concentration tested, swimming activity, as well as predator avoidance and endurance, were significantly reduced when measured as total distance swam during nonprovoked swimming (Fig. 1*C*, bar graph) and the number of lines crossed during a forced swim test (Fig. 1*C*, line graph), respectively. Minnows exposed to 0.26 μM TCS exhibited reduced nonprovoked and forced swimming behavior, although the magnitude of these impairments did not reach statistical significance (Fig. 1*C*).

TCS Impairs ECC in Vitro. The molecular mechanisms responsible for the impairments in muscle performance observed in vivo were investigated using primary cells isolated from murine cardiac and skeletal muscle. Cardiomyocytes were isolated from excised naive mouse hearts, loaded with the fluorescent Ca^{2+} indicator Fluo-4, and electrically paced at 1 Hz to evoke Ca^{2+} transients. After 20 min of exposure to 10 μM TCS, the evoked Ca^{2+} transients were greatly depressed with normalized peak amplitudes reduced by 79.3 ± 5.2% compared with cells exposed to equivalent vehicle as control (Fig. 2*A*). L-type Ca^{2+} entry through $Ca_v1.2$ (also termed the dihydropyridine receptor; DHPR) is essential for initiating cardiac ECC through a process termed Ca^{2+}-induced Ca^{2+}-release mediated as a consequence of RyR2 activation (25). Using the same TCS exposure protocol, voltage-clamped cardiomyocytes showed that 20 min after exposure to 10 μM TCS the peak L-type Ca^{2+} current was attenuated by 54.4 ± 9.6% compared with cardiomyocytes exposed to vehicle (Fig. 2*B*, *Center*), and the inactivation time constant was prolonged from 25.8 ± 2.0 ms to 45.2 ± 3.6 ms (Fig. 2*B*, *Right*).

The acute influences of TCS on ECC were assessed in more detail with mouse embryonic skeletal muscle cells (myotubes). Myotubes were stimulated with a standardized protocol that included electrical pulse trains ranging from 0.1 to 20 Hz over an ~30-min test period. As shown in Fig. 3*A* (*Top*), perfusion of vehicle had no measurable influence on the amplitude or kinetics of Ca^{2+} transients applied during the protocol. However, inclusion of TCS (0.5 μM) in the perfusate caused a gradual rise in baseline Ca^{2+} and significantly potentiated the maximum amplitude (corrected for baseline) of electrically evoked Ca^{2+} transients for the duration of the experiment (Fig. 3*A*, *Middle*). In contrast, 1 μM TCS initially potentiated Ca^{2+} transient amplitudes but invariably produced a subsequent diminution and eventual loss of electrically evoked Ca^{2+} transients (Fig. 3*A*, *Bottom*). The rapidity with which ECC was lost was highly dependent on the TCS concentration,

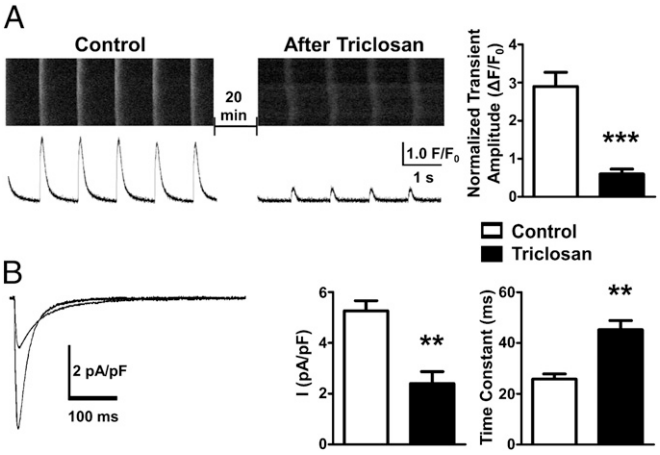

Fig. 2. TCS impairs cardiac ECC. (*A*) Isolated mouse cardiomyocytes ($n = 5$) were loaded with the fluorescent Ca^{2+} indicator Fluo-4. RyR2-mediated Ca^{2+} transients were evoked by field stimulation and measured by line-scan confocal imaging. Twenty minutes after applying 10 μM TCS, Ca^{2+} transient amplitudes were significantly reduced by 79.3 ± 5.2%. (*B*) Cardiomyocytes ($n = 5$) were patch-clamped in whole-cell configuration, and depolarized by voltage protocol. Exposure to 10 μM TCS for 20 min significantly reduced peak inward currents through $Ca_v1.2$ by 54.4 ± 9.6% and prolonged the inactivation time constant from 25.8 ± 2.0 ms to 45.2 ± 3.6 ms. All error bars represent SEM. $**P < 0.01$; $***P < 0.001$, *t* test.

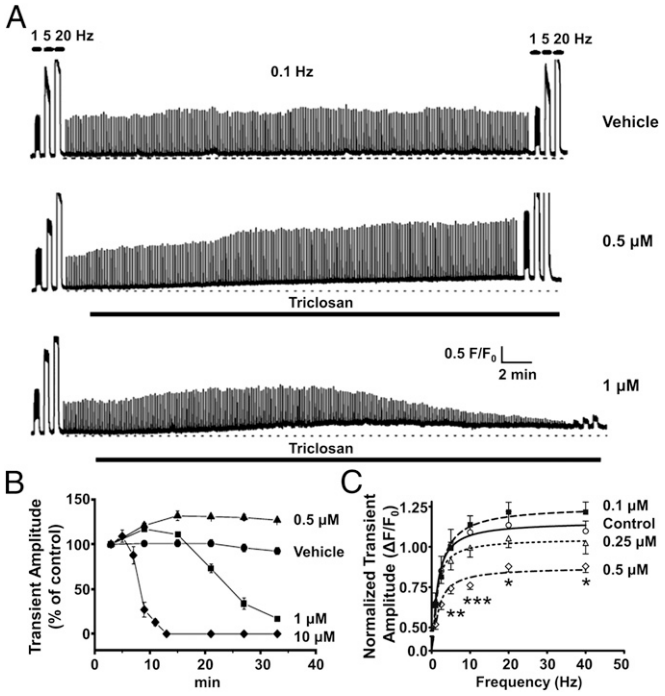

Fig. 3. TCS impairs skeletal ECC. (*A*) Mouse skeletal myotubes were loaded with the Ca^{2+} indicator Fluo-4 and electrically stimulated. Compared with vehicle (0.1% DMSO; *Top*) perfusion, 0.5 μM TCS significantly potentiated Ca^{2+} transient amplitudes (*Middle*). A similar potentiation was initially seen with 1 μM TCS, but this invariably led to the diminution and complete abrogation of electrically evoked Ca^{2+} transients (*Bottom*). (*B*) The effect of TCS on ECC is highly dose-dependent, with 10 μM causing rapid ECC failure within 12.5 min. All TCS exposures significantly altered the Ca^{2+} transient amplitude responses to single electrical test pulses ($P < 0.01$). Error bars represent SEM. (*C*) Exposure to submicromolar TCS for 24 h was sufficient to alter transient amplitudes in myotubes, with 0.5 μM TCS producing significant reductions at 5–40 Hz stimulus frequencies. Error bars represent SEM. *$P < 0.05$; **$P < 0.01$; ***$P < 0.001$, two-way ANOVA.

with 10 μM TCS causing a complete failure of ECC within ∼10 min (Fig. 3*B*; see also Fig. 6).

Myotubes exposed to TCS for 24 h before testing ECC revealed the drug's higher potency with longer (subacute) exposures. Exposure to as low as 0.1 μM TCS enhanced myotube Ca^{2+} transient amplitudes tested at ≥10 Hz stimuli, although this effect did not reach statistical significance. Nevertheless, TCS (0.5 μM) caused a significant depression of Ca^{2+} transient amplitudes at ≥5 Hz stimulus frequencies tested (Fig. 3*C*).

Acute exposure to TCS (10 μM) also caused a rapid failure of ECC in flexor digitorum brevis (FDB) muscle fibers isolated from adult mice (Fig. S2*A*), without causing either an initial increase in baseline Ca^{2+} or a potentiation of the Ca^{2+} transient amplitude, as was observed with myotubes. Subacute (24 h) exposure to lower TCS (0.5 μM) significantly reduced the number of responsive FDB fibers by 44.7 ± 8.6% (Fig. S2*B*).

TCS is known to tightly bind serum protein (2), and we therefore tested if the presence of BSA could prevent its acute actions on ECC in myotubes. BSA perfused in the imaging buffer at either 0.1% or 0.5% (final concentration) did not alter EC coupling responses (Fig. S3*A*). Even in the presence of 0.1% BSA, TCS (10 μM) impaired ECC in 67% of the cells (Fig. S3*B*), whereas TCS in the presence of 0.5% BSA impaired ECC in 22% of myotubes treated with 10 μM TCS (Fig. S3*C*). In all cases, however, serum albumin was unable to repress increases in resting Ca^{2+} levels, indicating that serum proteins alone cannot fully abate the adverse effects of TCS in myotubes.

In contrast to cardiac ECC, L-type Ca^{2+} entry through $Ca_v1.1$ is not required for initiating skeletal muscle ECC (26, 27). Instead, a form of conformational coupling engages bidirectional signaling between the voltage sensor of $Ca_v1.1$ and RyR1 activation (28, 29). Exposure to 10 μM TCS for 10 min before measuring Ca^{2+} current attenuated peak L-type Ca^{2+} current by nearly threefold compared with myotubes exposed to vehicle control (Fig. 4*B*, *Left*), and also caused a ∼fourfold acceleration of inactivation (Fig. 4*B*, *Right*). Although Ca^{2+} entry through $Ca_v1.1$ is not necessary to intially trigger ECC in skeletal muscle cells, the entry of Ca^{2+} through a mechanism requiring $Ca_v1.1$ appears to be essential for maintaining Ca^{2+} stores during prolonged physiological stimuli in a process termed excitation-coupled Ca^{2+} entry (ECCE) (30, 31). We therefore tested if TCS interfered with myotube ECCE using two approaches. First, ECCE was measured as the rate of quench of cytoplasmic fura-2 fluorescence as extracellular Mn^{2+} enters the myotube in response to a train of electrical pulses (40 Hz). As shown in Fig. 5*A*, 10 μM TCS caused a complete block of ECCE. Second, myotubes were pretreated with 500 μM ryanodine (30 min) to block RyR1, which was verified by the loss of responses to challenge with caffeine. In contrast to control cells that responded to a 40-Hz electrical pulse with a large Ca^{2+} entry, myotubes exposed to TCS (10 μM) failed to respond to an electrical pulse train (Fig. 5*B*). Importantly, inhibition of ECCE appears to be a selective action of TCS because it failed to inhibit store-operated Ca^{2+} entry (SOCE) subsequent to depletion of SR Ca^{2+} stores by thapsigargin (Fig. S4).

Molecular Targets of TCS-Mediated ECC Impairment. ECC in skeletal muscle invariably relies on bidirectional signaling between $Ca_v1.1$ and RyR1, which form a conformationally coupled unit. To further investigate whether TCS directly targets $Ca_v1.1$, RyR1, or both, we investigated its mechanism of action in wild-type and dyspedic (RyR1-null) myotubes. In addition to sequentially potentiating then blocking ECC, TCS (10 μM) caused a pronounced although transient rise in resting Ca^{2+} (Fig. 6*A*). After recovery to a slightly elevated baseline, brief challenge with caffeine (20 mM) produced a Ca^{2+} transient, the magnitude of which was not different compared with the caffeine response before TCS (area under curve = 72.5 ± 6.3 × 10^6 units before TCS treatment vs. 60.3 ± 8.3 × 10^6 units after TCS treatment; $n = 9$, $P = 0.26$), indicating that TCS causes ECC failure without depleting SR Ca^{2+} stores nor by block of RyR1 activity. Moreover, the loss of ECC in skeletal myotubes exposed to TCS was not the result of Na^+ channel block because depolarization of the myotube surface membrane with externally applied K^+ (40 mM) failed to elicit a Ca^{2+} transient (Fig. 6*A*, *Inset*). Dyspedic

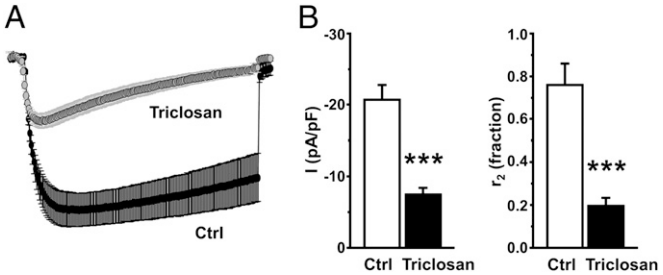

Fig. 4. TCS attenuates skeletal muscle L-type Ca^{2+} current. (*A*) Averaged recordings of L-type Ca^{2+} currents elicited by 2-s depolarizations from −50 mV to +30 mV are shown for untreated normal myotubes (black circle, $n = 4$) or normal myotubes exposed to 10 μM TCS for 15–20 min at ∼25 °C (gray circle, $n = 9$). (*B*) Summary of peak current densities (*Left*) and r_2 values (*Right*) for myotubes in the presence and absence of 10 μM TCS. r_2 is ratio of the current remaining at 2 s to the peak current. Error bars represent SEM. ***$P < 0.001$, *t* test.

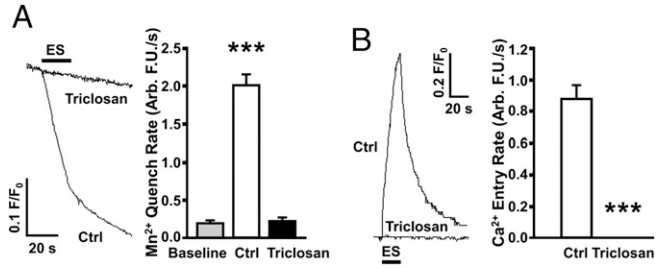

Fig. 5. TCS inhibits excitation-coupled Ca^{2+} entry. (*A*) The rate of ECCE was measured using Mn^{2+} quench of Fura-2 fluorescence at the isosbestic wavelength. Electrical stimuli (ES) were applied to myotubes perfused with 500 μM Mn^{2+}. Myotubes exposed to 10 μM TCS had negligible fluorescence quench compared with control, suggesting an inhibition of ECCE. (*B*) Ca^{2+} entry was monitored in ryanodine-treated myotubes loaded with the Ca^{2+} indicator Fluo-4. Ca^{2+} entry was induced by ES. Ryanodine-treated myotubes did not respond to caffeine, hence the rising signal represented pure ECCE, a process completely suppressed by 10 μM TCS. All error bars represent SEM. ***$P < 0.001$, *t* test.

myotubes did not respond to 10 μM TCS, as did RyR1-expressing myotubes (compare wild-type and dyspedic in Fig. 6*B*), indicating that TCS directly targeted RyR1 to produce a transient rise in baseline Ca^{2+}. In support of this interpretation, direct radioligand-receptor binding analysis showed that

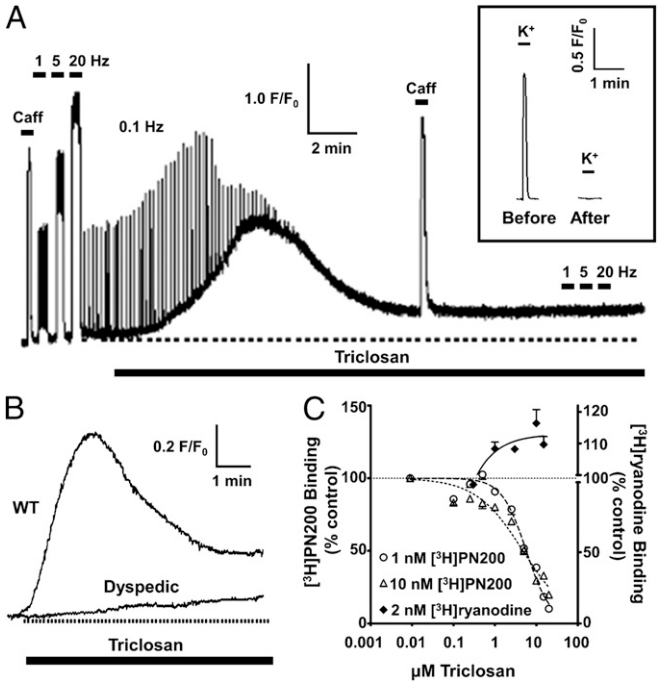

Fig. 6. TCS concomitantly affects both RyR and DHPR activity without depleting SR Ca^{2+} stores. (*A*) Mouse skeletal myotubes were loaded with the Ca^{2+} indicator Fluo-4 and electrically stimulated. Perfusion with 10 μM TCS resulted in a profound change in resting Ca^{2+}, as well as a rapid diminution and abrogation of Ca^{2+} transients. Challenge with 20 mM caffeine (Caff) indicates SR Ca^{2+} stores were not depleted. (*Inset*) In separate experiments, after TCS caused failure of myotubes to respond to electrical stimuli, challenge with 60 mM KCl (K^+) also failed to elicit ECC. (*B*) Dyspedic myotubes lacking RyR1 exhibited little change in cytosolic Ca^{2+} when exposed to TCS, implicating RyR1 as a molecular target of TCS. (*C*) Mouse skeletal muscle preparations were incubated with [^{3}H]ryanodine or [^{3}H]PN200 in the presence of TCS. TCS increased specific [^{3}H]ryanodine binding with respect to control, whereas specific [^{3}H]PN200 binding was inhibited noncompetitively across similar TCS concentrations.

TCS (1–20 μM) significantly enhanced specific [^{3}H]ryanodine binding to mouse skeletal muscle membrane preparations in a concentration-dependent manner (Fig. 6*C*). Specific binding of [^{3}H]PN200, a dihydropyridine that binds specifically to high-affinity sites on DHPR in skeletal muscle membrane preparations, was inhibited by TCS in a concentration-dependent but noncompetitive (allosteric) manner (Fig. 6*C*).

Discussion

We report that TCS is capable of disrupting ECC in both cardiac and skeletal muscle, resulting in impaired grip strength and hemodynamics, and mobility in a model fish species. These results were unexpected given the extensive toxicological testing of TCS recently reviewed (2). In fact, there is a dearth of information regarding the myotoxicity of TCS and its potential impacts on human and environmental health. An earlier study reported TCS to have an inhibitory effect on the excitability of rat phrenic nerve-diaphragm preparations; however, the mechanisms behind these findings were not explored and the study was largely ignored (32). Our present findings identify a potential for TCS to impair physiological muscle functions in vivo and identify proteins essential for ECC as targets, namely $Ca_v1.1$, $Ca_v1.2$, and RyR channels.

The molecular mechanisms by which TCS impairs ECC in skeletal muscle appear to stem from a unique functional dissociation (uncoupling) of bidirectional signaling between $Ca_v1.1$ and RyR1 Ca^{2+} release units (CRUs). Several observations support that TCS functionally disrupts ECC by selective interactions with the CRU: (*i*) TCS-induced failure of ECC is not associated with depletion of SR Ca^{2+} stores; (*ii*) TCS, even at high concentration (10 μM), fails to block RyR1 channels (myotubes remain responsive to caffeine and [^{3}H]ryanodine binding is enhanced); (*iii*) The loss of ECC can be demonstrated even with external additions of K^+ to depolarize the myotubes, which bypasses the Na^+ action potential; (*iv*) TCS influences [^{3}H]PN200 binding to DHPR in a noncompetitive manner and enhances [^{3}H]ryanodine binding to RyR1 in the same concentration range; (*v*) The TCS-modified skeletal L-type Ca^{2+} current is reduced in density; (*vi*) The transient rise in basal Ca^{2+} caused by TCS is dependent on RyR1 expression and tightly coincides with loss of ECC and ECCE, but not SOCE, suggesting that TCS influences both proteins at sites critical for CRU interactions. Regardless of the exact molecular mechanisms leading to loss of CRU function, impairment of bidirectional signaling in even a fraction of skeletal muscle CRUs would be expected to result in weakened contractility, promoting fatigue, sarcopenia, or cachexia, a conclusion verified in grip-strength measurements made following acute exposure to TCS. Prolonged increases in cytosolic Ca^{2+} have been shown to promote contractile fatigue in adult skinned muscle fibers and ECC failure (33, 34). Our current results in adult FDB fibers and myotubes indicate that at lower concentrations (≤1 μM) of TCS impairs CRU functions without overtly promoting chronically elevated cytoplasmic Ca^{2+}, suggesting TCS-mediated CRU dysfunction is mediated by a unique mechanism that chemically interferes with CRU function.

TCS also interferes with cardiac ECC, even though cardiac CRUs have fundamental differences in physical organization and functional coupling between $Ca_v1.2$ and RyR2. The activation of RyR2 depends solely on Ca^{2+} entry through $Ca_v1.2$, and block of Ca^{2+} entry prevents RyR2-mediated Ca^{2+} release. Because TCS reduces $Ca_v1.2$ current by ∼50%, direct block of L-type Ca^{2+} current may represent the primary mechanism by which TCS impairs cardiac ECC. TCS also retards inactivation of $Ca_v1.2$, an action that is likely secondary to Ca^{2+} transient attenuation, because RyR2-mediated Ca^{2+} release from the SR plays major feedback role in the inactivation of L-type Ca^{2+} current (35). Indeed, the in vitro effects of TCS on cardiac ECC are further supported by the in vivo analyses using hemody-

namic monitoring. TCS results in a suppression of the maximal left ventricular pressure development in a dose-dependent manner. This effect is associated with a significant reduction in cardiac output.

Dysregulation of cardiac ECC has been implicated in heart failure, cardiac arrhythmias, and cardiomyopathies (36). A prominent comorbidity of heart failure with poor prognosis is cachexia (37). TCS-mediated ECC failure could promote adverse cardiac outcomes, especially in such susceptible populations with mutations in CRU proteins known to confer stress-triggered arrhythmias.

Commensurate with the increased production of TCS over the past four decades (1–3) are increased exposures, as evidenced in human samples of urine, plasma, and breast milk (7–9). Typical routes of exposure to TCS (oral, dermal) are sufficient in bringing the compound into systemic circulation (38, 39). Importantly, one study reported plasma C_{max} of nearly 1 μM within 1–3 h after administering a 4-mg oral dose in human subjects (38). Our acute in vivo experiments were aimed at understanding mechanisms and potential risks, and therefore used an intraperitoneal route of exposure. However, the exposures tested here produced TCS blood plasma concentrations consistent with levels found in some humans. Therefore, disruption of ECC in skeletal and cardiac muscle may also inform about previously unappreciated risk factors associated with pervasive exposures to TCS in both humans and environmentally sensitive species (e.g., fish). TCS has been detected in sewage sludge and sediment, as well as in organisms ranging from algae to fish to dolphins (3, 6). Using fathead minnows as a marker for aquatic toxicology, Schultz et al. recently reported that TCS decreased aggression and predator-avoidance performance in the minnow (40). Consistent with this report, our study revealed a negative impact on swimming performance in larval fathead minnows exposed to TCS, an effect attributable to perhaps a combination of both cardiac and skeletal muscle impairments. In this regard, recent studies have found TCS in both raw and treated drinking water, as well as in >60% of streams across 30 states (1, 4, 5), suggesting that ecosystems are also impacted by exposure to this high-volume chemical.

In mammals, TCS is primarily metabolized to glucuronide and sulfate conjugates, yet details regarding the extent of conjugation have been equivocal. Reports about human exposure range from very little or no detectable levels of parent compound to 38% unconjugated after oral ingestion of TCS (2, 38, 41). The basis for this discrepancy is not known, but a possible explanation may involve disparate glucuronidation or sulfation capacities in the subjects tested. Indeed, UDP-glucuronosyltransferases are highly polymorphic (42) and genetic disorders, like Gilbert-Meulengracht syndrome, which affects 5–10% of the population, can lead to decreased UDP-glucuronosyltransferase activity (43). Overall, these genetic variations could dramatically influence the capacity to clear TCS from systemic circulation by conjugation. Thus, a segment of the human population with impaired phase II metabolism might be at a higher risk of adverse TCS effects described in this article. Plasma protein binding has been suggested to mitigate the possible effects of TCS, because more than 95% of the compound is protein-bound in human blood (2). However, our results demonstrated that TCS disrupts skeletal ECC even in the presence of excess serum protein.

In conclusion, we show that TCS potently impairs striated muscle ECC by interfering with signaling between DHPR and RyR, resulting in weakened contractility and depressed hemodynamics. Considering that exposures to TCS are pervasive, these recent finding may present a concern to both human and environmental health.

Materials and Methods

More detailed descriptions can be found in *SI Materials and Methods*.

Animal Use. All mouse and fathead minnow experiments were conducted under protocols approved by the Institutional Animal Care and Use Committee at the University of California at Davis.

Hemodynamic Measurement. Hemodynamic measurements were performed as described previously (44). After signal stabilization for 10–15 min, the baseline pressure-volume (PV) loops at a steady state were recorded followed by intraperitoneal administration of 6.25, 12.5, or 25 mg/kg of TCS or vehicle. PV loops were recorded after 15 min of drug administration. A stock of TCS was prepared in DMSO and diluted [20% (vol/vol)] into saline to give a total volume of 200 μL before injection.

Determination of TCS Concentration in Mouse Plasma. Fifteen minutes after intraperitoneal administration of TCS to mice, blood was collected by cardiac puncture and directly processed to plasma by centrifugation. TCS levels in plasma were determined by liquid chromatography electrospray-ionization tandem mass spectrometry with online solid-phase extraction, as previously described (45).

Mouse in Vivo Grip Strength. Grip strength was measured with 3-mo-old wild-type male C57BL/6 mice using a grip-strength meter with metal wire mesh (Columbus Instruments). Upon acquiring baseline readings, the mice were administered sham, vehicle, or 40 mg/kg TCS by intraperitoneal injection, and grip strength was evaluated up to 1 h. Sham, vehicle, and TCS groups were compared via one-way ANOVA with Newman-Keuls posttest using Prism (GraphPad Software).

Swimming Behavior in Larval Fathead Minnow. Larval fathead minnow (Aquatox, Inc.), 7 d posthatch, were exposed for up to 7 d to dilution water, 0.01% methanol, or 0.035, 0.26, and 0.52 μM TCS in 0.01% methanol. Control and dilution water consisted of deionized water, modified to USEPA moderately hard standards (46), and tests followed standard USEPA (46, 47) protocols. Swimming behavior was assessed in two stages: (*i*) nonprovoked swimming activity captured using video monitoring and analyzed using Ethovision Behavior Software (Noldus Information Technology); (*ii*) provoked swimming behavior techniques designed by Heath et al. (48) as described by Beggel and colleagues (49). All time points were combined (n = 36) by concentration for each swimming parameter (n = 36) and effects were determined using a Kruskal-Wallis followed by a Dunn's posttest.

Isolation of Adult Mouse Ventricular Myocytes. Single-mouse free-wall left ventricular myocytes were isolated from 10- to 12-wk-old C57BL/6J mice, as previously described (50).

Confocal Ca^{2+} Imaging of Mouse Ventricular Myocytes. Ca^{2+} responses from isolated left ventricular myocytes were evoked and measured, as previously described (51).

Measurement of Cardiac L-type Ca^{2+} Current. L-type currents were recorded from isolated left ventricular myocytes, as previously described (52).

Preparation and Culture of Primary Myotubes and Adult FDB Fibers. Primary skeletal myoblasts were isolated from wild-type and dyspedic (RyR1-null) mouse neonates and cultured, as previously described (31). FDB muscles were dissected from 3- to 6-mo-old WT male mice, and single myofibers were enzymatically isolated and cultured, as previously described (53).

Imaging of Primary Myotubes and Adult FDB Fibers. Ca^{2+} responses from myotubes and FDB fibers were evoked and measured, as previously described (54).

Measurement of Skeletal L-type Ca^{2+} Current. L-type currents were recorded from skeletal myotubes as described previously (55).

Preparations of Membrane Fractions from Mouse Skeletal Muscle. SR microsomes were isolated from mouse skeletal muscle tissue, as previously described (54).

Radioligand Binding Assay. Radioligand binding assays with [^{3}H]ryanodine and [^{3}H]PN200 were performed as previously described (54, 56).

Statistical Analysis. All data are presented as mean ± SEM. All comparisons were made by two-tailed unpaired t test unless otherwise indicated; $P < 0.05$ was considered significant.

ACKNOWLEDGMENTS. This work was supported by National Institutes of Health Grants 1P01 AR52354 (to I.N.P. and K.G.B.), 2P01 ES011269 (to I.N.P.), P42 ES004699 (to B.D.H., I.N.P., and N.C.), R03 AG038778 (to R.A.B), R01 AR055104 (to K.G.B.), R01 ES002710 (to B.D.H.), and R01 HL85727, R01 HL85844, and VA Merit Grant 5 I01BX000576 (to N.C.); Muscular Dystrophy Association Grants 176448 (to K.G.B.) and T32 HL86350 (to R.Z.); and the J. B. Johnson Foundation (I.N.P.). B.D.H. is a George and Judy Marcus Senior Fellow of the American Asthma Society.

1. Fang JL, et al. (2010) Occurrence, efficacy, metabolism, and toxicity of triclosan. *J Environ Sci Health C Environ Carcinog Ecotoxicol Rev* 28:147–171.
2. Rodricks JV, Swenberg JA, Borzelleca JF, Maronpot RR, Shipp AM (2010) Triclosan: A critical review of the experimental data and development of margins of safety for consumer products. *Crit Rev Toxicol* 40:422–484.
3. Dann AB, Hontela A (2011) Triclosan: Environmental exposure, toxicity and mechanisms of action. *J Appl Toxicol* 31:285–311.
4. Loraine GA, Pettigrove ME (2006) Seasonal variations in concentrations of pharmaceuticals and personal care products in drinking water and reclaimed wastewater in southern California. *Environ Sci Technol* 40:687–695.
5. Kolpin DW, et al. (2002) Pharmaceuticals, hormones, and other organic wastewater contaminants in U.S. streams, 1999–2000: A national reconnaissance. *Environ Sci Technol* 36:1202–1211.
6. Chu S, Metcalfe CD (2007) Simultaneous determination of triclocarban and triclosan in municipal biosolids by liquid chromatography tandem mass spectrometry. *J Chromatogr A* 1164:212–218.
7. Calafat AM, Ye X, Wong LY, Reidy JA, Needham LL (2008) Urinary concentrations of triclosan in the U.S. population: 2003–2004. *Environ Health Perspect* 116:303–307.
8. Hovander L, et al. (2002) Identification of hydroxylated PCB metabolites and other phenolic halogenated pollutants in human blood plasma. *Arch Environ Contam Toxicol* 42:105–117.
9. Adolfsson-Erici M, Pettersson M, Parkkonen J, Sturve J (2002) Triclosan, a commonly used bactericide found in human milk and in the aquatic environment in Sweden. *Chemosphere* 46:1485–1489.
10. Stoker TE, Gibson EK, Zorrilla LM (2010) Triclosan exposure modulates estrogen-dependent responses in the female wistar rat. . *Toxicol Sci* 117(1):45–53.
11. Clayton EM, Todd M, Dowd JB, Aiello AE (2011) The impact of bisphenol A and triclosan on immune parameters in the U.S. population, NHANES 2003–2006. *Environ Health Perspect* 119:390–396.
12. Morisseau C, et al. (2009) Toxicology in the fast lane: Application of high-throughput bioassays to detect modulation of key enzymes and receptors. *Environ Health Perspect* 117:1867–1872.
13. Pannu MW, O'Connor GA, Toor GS (2012) Toxicity and bioaccumulation of biosolids-borne triclosan in terrestrial organisms. *Environ Toxicol Chem* 31:646–653.
14. Russell AD (2004) Whither triclosan? *J Antimicrob Chemother* 53:693–695.
15. Zorrilla LM, et al. (2009) The effects of triclosan on puberty and thyroid hormones in male Wistar rats. *Toxicol Sci* 107(1):56–64.
16. Ahn KC, et al. (2008) In vitro biologic activities of the antimicrobials triclocarban, its analogs, and triclosan in bioassay screens: Receptor-based bioassay screens. *Environ Health Perspect* 116:1203–1210.
17. Pessah IN, et al. (2006) Structure-activity relationship for noncoplanar polychlorinated biphenyl congeners toward the ryanodine receptor-Ca2+ channel complex type 1 (RyR1). *Chem Res Toxicol* 19:92–101.
18. Kim KH, et al. (2011) Para- and ortho-substitutions are key determinants of polybrominated diphenyl ether activity toward ryanodine receptors and neurotoxicity. *Environ Health Perspect* 119:519–526.
19. Pessah IN, Lynch, C, 3rd, Gronert GA (1996) Complex pharmacology of malignant hyperthermia. *Anesthesiology* 84:1275–1279.
20. Zhou J, Allen PD, Pessah IN, Naguib M (2010) *Miller's Anesthesia* (Churchill Livingstone, Philadelphia, PA), 7th Ed.
21. Andersson DC, et al. (2011) Ryanodine receptor oxidation causes intracellular calcium leak and muscle weakness in aging. *Cell Metab* 14:196–207.
22. Priori SG, Chen SR (2011) Inherited dysfunction of sarcoplasmic reticulum Ca2+ handling and arrhythmogenesis. *Circ Res* 108:871–883.
23. Shan J, et al. (2010) Role of chronic ryanodine receptor phosphorylation in heart failure and β-adrenergic receptor blockade in mice. *J Clin Invest* 120:4375–4387.
24. Ankley GT, Villeneuve DL (2006) The fathead minnow in aquatic toxicology: past, present and future. *Aquat Toxicol* 78:91–102.
25. Bers DM (2002) Cardiac excitation-contraction coupling. *Nature* 415:198–205.
26. Gonzalez-Serratos H, Valle-Aguilera R, Lathrop DA, Garcia MC (1982) Slow inward calcium currents have no obvious role in muscle excitation-contraction coupling. *Nature* 298:292–294.
27. Armstrong CM, Bezanilla FM, Horowicz P (1972) Twitches in the presence of ethylene glycol bis(-aminoethyl ether)-N,N′-tetracetic acid. *Biochim Biophys Acta* 267:605–608.
28. Nakai J, et al. (1996) Enhanced dihydropyridine receptor channel activity in the presence of ryanodine receptor. *Nature* 380:72–75.
29. Tanabe T, Beam KG, Powell JA, Numa S (1988) Restoration of excitation-contraction coupling and slow calcium current in dysgenic muscle by dihydropyridine receptor complementary DNA. *Nature* 336:134–139.
30. Bannister RA, Pessah IN, Beam KG (2009) The skeletal L-type Ca(2+) current is a major contributor to excitation-coupled Ca(2+) entry. *J Gen Physiol* 133:79–91.
31. Cherednichenko G, et al. (2004) Conformational activation of Ca2+ entry by depolarization of skeletal myotubes. *Proc Natl Acad Sci USA* 101:15793–15798.
32. Kjaerheim V, Röed A, Brodin P, Rölla G (1995) Effects of triclosan on the rat phrenic nerve-diaphragm preparation. *J Clin Periodontol* 22:488–493.
33. Verburg E, Dutka TL, Lamb GD (2006) Long-lasting muscle fatigue: Partial disruption of excitation-contraction coupling by elevated cytosolic Ca2+ concentration during contractions. *Am J Physiol Cell Physiol* 290:C1199–C1208.
34. Lamb GD, Junankar PR, Stephenson DG (1995) Raised intracellular [Ca2+] abolishes excitation-contraction coupling in skeletal muscle fibres of rat and toad. *J Physiol* 489:349–362.
35. Dirksen RT (2002) Bi-directional coupling between dihydropyridine receptors and ryanodine receptors. *Front Biosci* 7:d659–d670.
36. Wehrens XH, Lehnart SE, Marks AR (2005) Intracellular calcium release and cardiac disease. *Annu Rev Physiol* 67:69–98.
37. Anker SD, Steinborn W, Strassburg S (2004) Cardiac cachexia. *Ann Med* 36:518–529.
38. Sandborgh-Englund G, Adolfsson-Erici M, Odham G, Ekstrand J (2006) Pharmacokinetics of triclosan following oral ingestion in humans. *J Toxicol Environ Health A* 69:1861–1873.
39. Queckenberg C, et al. (2010) Absorption, pharmacokinetics, and safety of triclosan after dermal administration. *Antimicrob Agents Chemother* 54:570–572.
40. Schultz MM, Bartell SE, Schoenfuss HL (2012) Effects of triclosan and triclocarban, two ubiquitous environmental contaminants, on anatomy, physiology, and behavior of the fathead minnow (*Pimephales promelas*). *Arch Environ Contam Toxicol* 63:114–124.
41. Lin YJ (2000) Buccal absorption of triclosan following topical mouthrinse application. *Am J Dent* 13:215–217.
42. Miners JO, McKinnon RA, Mackenzie PI (2002) Genetic polymorphisms of UDP-glucuronosyltransferases and their functional significance. *Toxicology* 181-182:453–456.
43. Strassburg CP (2010) Hyperbilirubinemia syndromes (Gilbert-Meulengracht, Crigler-Najjar, Dubin-Johnson, and Rotor syndrome). *Best Pract Res Clin Gastroenterol* 24: 555–571.
44. Pacher P, Nagayama T, Mukhopadhyay P, Bátkai S, Kass DA (2008) Measurement of cardiac function using pressure-volume conductance catheter technique in mice and rats. *Nat Protoc* 3:1422–1434.
45. Schebb NH, et al. (2011) Investigation of human exposure to triclocarban after showering and preliminary evaluation of its biological effects. *Environ Sci Technol* 45: 3109–3115.
46. USEPA (2002) *Short-Term Methods for Estimating the Chronic Toxicity of Effluents and Receiving Waters to Freshwater Organisms* (US Environmental Protection Agency, Washington, DC).
47. USEPA (2002) *Methods for Measuring the Acute Toxicity of Effluents and Receiving Waters to Freshwater Organisms* (US Environmental Protection Agency, Washington, DC).
48. Heath AG, Cech JJ, Jr., Zinkl JG, Steele MD (1993) Sublethal effects of three pesticides on Japanese medaka. *Arch Environ Contam Toxicol* 25:485–491.
49. Beggel S, Werner I, Connon RE, Geist JP (2010) Sublethal toxicity of commercial insecticide formulations and their active ingredients to larval fathead minnow (*Pimephales promelas*). *Sci Total Environ* 408:3169–3175.
50. Li N, et al. (2009) Ablation of a Ca2+-activated K+ channel (SK2 channel) results in action potential prolongation in atrial myocytes and atrial fibrillation. *J Physiol* 587:1087–1100.
51. Xu Y, et al. (2005) The effects of intracellular Ca2+ on cardiac K+ channel expression and activity: Novel insights from genetically altered mice. *J Physiol* 562:745–758.
52. Zhang Z, et al. (2002) Functional Roles of $Ca_{(v)}1.3$ ($\alpha_{(1D)}$) calcium channel in sinoatrial nodes: Insight gained using gene-targeted null mutant mice. *Circ Res* 90:981–987.
53. Brown LD, Rodney GG, Hernández-Ochoa E, Ward CW, Schneider MF (2007) Ca2+ sparks and T tubule reorganization in dedifferentiating adult mouse skeletal muscle fibers. *Am J Physiol Cell Physiol* 292:C1156–C1166.
54. Feng W, et al. (2011) Functional and biochemical properties of ryanodine receptor type 1 channels from heterozygous R163C malignant hyperthermia-susceptible mice. *Mol Pharmacol* 79:420–431.
55. Eltit JM, et al. (2012) Malignant hyperthermia susceptibility arising from altered resting coupling between the skeletal muscle L-type Ca2+ channel and the type 1 ryanodine receptor. *Proc Natl Acad Sci USA* 109:7923–7928.
56. Buck ED, Nguyen HT, Pessah IN, Allen PD (1997) Dyspedic mouse skeletal muscle expresses major elements of the triadic junction but lacks detectable ryanodine receptor protein and function. *J Biol Chem* 272:7360–7367.

Supporting Information

Cherednichenko et al. 10.1073/pnas.1211314109

SI Materials and Methods

Hemodynamic Measurement. Hemodynamic measurement was performed as described previously (1). In brief, 8- to 10-wk-old male C57BL/6J mice were anesthetized with ketamine/xylazine (80 and 5 mg/kg, respectively). The neck and chest area was shaved and mice were carefully moved to the heating pad with a servo-controlled homeothermic blanket using a rectal temperature feedback probe. The desired body temperature was set to 37 °C. An inverted T-shaped middle-neck incision from mandible to the sternum was made. The parotid glands were moved aside and blunt dissection of the thin muscle layer around the throat was performed to expose and isolate the right carotid artery. The carotid artery was separated from the vagus nerve and a miniature pressure-volume (PV) catheter (SPR-839; Millar Instruments) was inserted via the carotid artery tip into the left ventricle. The PV signals were acquired using the Millar PV system (MPVS-300, PowerLab 4/30 with Chart Pro; AD Instruments). After stabilization of the signal for 10–15 min, the baseline PV [loops at a steady state were recorded followed by intraperitoneal administration of 100, 50, 25, or 12.5 mg/kg of triclosan (TCS) or vehicle]. PV loops were recorded after 15 min of drug administration. A stock of TCS was prepared in DMSO and diluted [20% (vol/vol)] into saline to give a total volume of 200 μL before injection. Before and after treatment, measurements were compared using one-tailed paired *t* tests.

Determination of TCS Concentration in Mouse Plasma. TCS analysis was performed by online solid-phase extraction (SPE)-LC-MS on an Agilent 1200 LC system coupled to a ABI 4000 TRAP tandem mass spectrometer (MS/MS) equipped with a pneumatically assisted electrospray-ionization (ESI) source (Applied Biosystems). The SPE-LC analysis was carried out as described for triclocarban (2), using a Cyclone RP-18 column (50 × 0.5 mm, 50 μm; Thermo Fisher Scientific) as SPE column and a Kinetex C18 reverse-phase separation column (50 × 2.1 mm, 10 nm; Phenomenex). Separation was carried out with water containing 25 mM ammonium acetate and 0.1% acetic acid as solvent A and acetonitrile/water [95%/5% (vol/vol)] as solvent B. The flow rate for separation was set to 350 μL/min and the following gradient was used: 0.0–0.5 min isocratic 55% B; 0.5–0.7 min linear from 55% B to 100% B; 0.7–1.8 min isocratic 100% B and return to initial conditions at 1.9 min. TCS and its internal standard (IS) $^{2}H_{3}$-TCS were detected after negative ESI in selected reaction monitoring mode on the transitions of *m/z* 287/35 and *m/z* 292/35 with a dwell time of 50 ms. The instrument was operated with an ion-spray voltage of −4,500 V, using 25 psi curtain gas, 40 psi nebulizer gas, and 71 psi drying gas at a temperature of 500 °C and collision energy of −42 V.

Sample preparation was carried out by mixing mouse plasma with IS solution in ACN yielding a final IS concentration of 50 nM. Following mixing and centrifugation (14,000 × *g* for 4 min at 4 °C), 20 μL of the mixture were directly analyzed by online-SPE-LC-MS.

TCS coeluted perfectly with the IS at a retention time of 1.51 ± 0.03 min in narrow peaks (full-width at half-maximum height 0.06 ± 0.01 min). The limit of detection for TCS was 0.1 nM (2 fmol on column) with a linear dynamic detection range from 0.3 to 600 nM TCS. The method showed a very good accuracy and precision in spiked plasma samples (recovery rate 100 ± 15% of the spiked concentration, intrasample variation ≤ 5%, intersample variation ≤ 10%).

Mouse in Vivo Grip Strength. Three-month-old wild-type male C57BL/6 mice (~25 g) were acclimated to laboratory conditions for 2 d before grip-strength evaluation using a grip-strength meter with metal wire mesh (Columbus Instruments). Mice were randomly assigned to DMSO vehicle ($n = 7$) and 40 mg/kg TCS ($n = 8$) groups. To measure grip strength, mice were allowed to grab onto the wire mesh with all four limbs and gently pulled away from the meter by the base of the tail using a smooth horizontal motion. Before dosing, baseline grip strength was assessed for each mouse over a 30-min period, with five readings performed every 10 min. Mice were dosed via intraperitoneal injection, with dose volume not exceeding 30 μL. The evaluator was blind to the dose received by each mouse. Following injection, the grip strength for each mouse was evaluated up to 1 h, with five readings performed every 10 min. Sham injections were performed on a separate group of seven mice, and grip strength was evaluated following the same time course. Baseline measurements for each mouse were averaged, excluding the two highest and two lowest readings. Postdose measurements were averaged and expressed as a percent of baseline for each mouse. Nonresponders to TCS were determined as $P > 0.05$ when comparing baseline and postdose mean grip strength by *t* test and excluded from final analysis ($n = 1$). Sham, vehicle, and TCS groups were compared via one-way ANOVA with Newman-Keuls posttest using Prism (GraphPad Software).

Swimming Behavior in Larval Fathead Minnow. Larval fathead minnow (Aquatox), 7 d posthatch at test initiation, were exposed for up to 7 d to control water, a 0.01% methanol solvent control, or 10, 75, or 150 μg/L (0.035, 0.26, 0.52 μM, respectively) TCS in 0.01% methanol. Control and dilution water consisted of deionized water, modified to US Environmental Protection Agency (USEPA) moderately hard standards (3). Furthermore, all tests followed standard USEPA protocols (3, 4). For each treatment there were a total of 12 replicate beakers of 10 fish and each beaker contained 250 mL of exposure solution. During the exposure fish were feed three times daily with 300–500 *Artemia franciscana* nauplii and exposed to 16:8 light:dark photoperiod. Fish were not feed for at least 12 h before test termination and subsequent swimming analysis.

After 1, 4, or 7 d of exposure 12 fish from each treatment, three from each of four replicate beakers, underwent swimming analysis. The remainder of the fish per replicate beaker was euthanized using an overdose of tricaine methanesulfonate (Argent Chemical Laboratories). Swimming behavior was assessed in two stages: (*i*) nonprovoked swimming behavior to assess normal swimming activity, and (*ii*) forced swimming behavior designed to assess predator avoidance and swimming endurance (5). Individual fish were randomly selected, placed into a swimming apparatus containing control water, and allowed to acclimate for at least 60 s. Nonprovoked swimming analysis was captured using overhead video monitoring and later analyzed for total distance traveled within 80 s using Ethovision Behavior Software (Noldus Information Technology). To assess predator avoidance and endurance the race-track method described by Heath et al. (5) was used. Briefly, fish were placed into a circular racetrack divided into eight equidistant sections and provoked by gentle touches to the tail fin with a glass pipette. The fish was provoked every time they stopped swimming and the number of lines crossed within 60 s was recorded (6).

To describe TCS's effect on the swimming behavior in larval fish, all time points were combined ($n = 36$) by concentration for

each swimming parameter. Data collected for provoked swimming analysis did not fit the assumption of equal variance for an ANOVA and therefore all data were assessed using a Kruskal-Wallis followed by a Dunn's posttest. It should be mentioned that data were also assessed using an ANOVA blocked by time of exposure and showed consistent results; therefore, the more conservative results from the nonparametric analyses were used.

Isolation of Adult Mouse Ventricular Myocytes. Single-mouse free-wall left ventricular myocytes were isolated from 10- to 12-wk-old C57BL/6J mice as previously described (7, 8). In brief, mice were injected with 0.1 mL heparin (1,000 units/mL) and after 5 min anesthetized with intraperitoneal sodium pentobarbital (40 mg/kg). Hearts were quickly removed and placed in ice-cold Tyrode's solution (NaCl 140 mM, KCl 5.4 mM, $MgCl_2$ 1 mM, Hepes 10 mM, and glucose 10, pH 7.4), cannulated under a dissecting microscope and mounted on a Langendorff apparatus. Perfusion of hearts was done with Tyrode's solution gassed with 100% O_2 at 37 °C under constant perfusion pressure (60 mmHg) and a flow rate of ~2 mL/min. After 5 min, solution was changed to 30 mL of Tyrode's solution containing 13 mg collagenase (type 2, 322 units/mg; Worthington Biochemical Corporation) and 1 mg protease (type XIV, 4.5 units/mg; Sigma-Aldrich). Hearts were removed from the Langendorff apparatus after 30–45 min of enzyme perfusion. Ventricular tissues were collected in high-K^+ solution (K glutamate 120 mM, KCl 20 mM, $MgCl_2$ 1 mM, EGTA 0.3 mM, glucose 10 mM, and Hepes 10 mM, pH 7.4), and gently triturated with pipettes for 3 min. Because of the known electrophysiological heterogeneity in various regions of the heart, we used only left ventricular free-wall cells for our recordings. Cells were allowed to rest for 2 h before use. This isolation procedure yielded 60–80% of Ca^{2+} tolerant ventricular myocytes with clear striation.

Confocal Ca^{2+} Imaging of Mouse Ventricular Myocytes. Enzymatically isolated free-wall left ventricular myocytes were loaded with the Ca^{2+} indicator Fluo-4 (9, 10). Cells were field-stimulated at a frequency of 1 Hz (IonOptix). Confocal line-scan imaging was performed by using a Zeiss Pascal confocal microscope equipped with an argon laser (488 nm) and a 40×, 1.3 N.A. oil immersion objective lens. Line-scan images were acquired at sampling rates of 0.7 ms per line and 0.07 μm per pixel, with radial and axial resolutions of 0.4 and 1.0 μm, respectively. Ca^{2+} transients were expressed as the normalized local fluorescence (F/F_0), where F_0 refers to the fluorescence level before depolarization, as previously described (9, 10). Ca^{2+} signals were measured before and 20 min after perfusion of TCS (10 μM) to myocytes. Where appropriate, pooled data are presented as means ± SEM. Significant differences between groups were determined by *t* test.

Measurement of Cardiac L-Type Ca^{2+} Current. Whole-cell L-type Ca^{2+} currents were recorded at room temperature by using patch-clamp techniques as previously described (11, 12). The external solution contained: *N*-methyl-D-glucamine 140 mM, CsCl 5 mM, $MgCl_2$ 0.5 mM, $CaCl_2$ 2 mM, 4-aminopyridine 2 mM, glucose 10 mM, and Hepes 10 mM, pH 7.4, and the internal solution contained: CsCl 125 mM, tetraethylammonium chloride 20 mM, Mg-ATP 4 mM, BAPTA 0.05 mM, and Hepes 10 mM, pH 7.3. All experiments were performed using 3 M KCl agar bridges. Cell capacitance was calculated as the ratio of net charge (the integrated area under the current transient) to the magnitude of the pulse (20 mV). Currents were normalized to cell capacitance to obtain the current density. The series resistance was compensated electronically. In all experiments, a series resistance compensation of ≥90% was obtained. Currents were recorded using Axopatch 200B amplifier (Axon Instrument), filtered at 2 kHz using a four-pole Bessel filter and digitized at sampling frequency of 10 kHz. L-type Ca^{2+} currents were measured before and 20 min after perfusion of TCS (10 μM) to myocytes. Data analysis was carried out using custom-written software and commercially available PC-based spreadsheet and graphics software (OriginPro 7; OriginLab).

Preparation and Culture of Primary Myotubes and Adult Flexor Digitorum Brevis Fibers. Primary skeletal myoblasts were isolated from WT and dyspedic (RyR1-null) mouse neonates and expanded onto 96-well microclear plates (BD Falcon) coated with Matrigel (BD Biosciences), as previously described (13). Upon reaching 60% confluence, growth factor was withdrawn and the cells were allowed to differentiate into myotubes for 3–5 d in DMEM (Invitrogen) containing 5% heat-inactivated horse serum and 2 mM L-glutamine.

Flexor digitorum brevis (FDB) muscles were dissected from 3- to 6-mo-old wild-type male mice, and single myofibers were enzymatically isolated, as previously described (14). After isolation, the fibers were plated onto Matrigel-coated plates and cultured in DMEM containing 10% FBS and penicillin-streptomycin at 37 °C. Experiments were conducted within 12–40 h of plating.

Imaging of Primary Myotubes and Adult FDB Fibers. Ca^{2+} responses from myotubes and FDB fibers were evoked and measured as previously described (15). Briefly, myotubes or FDB fibers were loaded with the Ca^{2+} indicator Fluo-4 and imaged using an intensified charge coupled device camera with a 40× objective. Data were collected from 3 to 10 individual cells at ≥ six frames per second. TCS (0.5–10 μM) was delivered to the cells by bulk perfusion, and Ca^{2+} transients were evoked by electrical field stimulation using two platinum electrodes attached to opposite sides of the well and connected to a stimulator that delivered a range of frequencies (0.1–20 Hz). The cells were challenged by caffeine through a brief puff delivered by micropipette. For TCS pretreatment, myotubes and fibers were incubated for 24 h in serum-free DMEM. Frequency-amplitude measurements were curve-fit by nonlinear regression using Prism (GraphPad Software) and analyzed by two-way ANOVA with Bonferroni posttests. For certain experiments, 0.1–0.5% BSA was added to the buffer and perfused to myotubes in addition to TCS.

Store-operated Ca^{2+} entry (SOCE) and excitation-coupled Ca^{2+} entry (ECCE) measurements were performed as previously described (13, 16). To assess SOCE, myotubes were loaded with Fluo-4 and treated with thapsigargan through perfusion in a Ca^{2+}-free buffer. After Ca^{2+} mobilization, 10 μM TCS was added to the perfusion buffer, and Ca^{2+} entry was measured through reintroduction of extracellular Ca^{2+}. ECCE was assessed using Mn^{2+} quench of Ca^{2+}-insensitive Fura-2 fluorescence, as well as increase in Ca^{2+}-sensitive Fluo-4 fluorescence. For Mn^{2+} quench, cells were perfused with 500 μM extracellular Mn^{2+} and illuminated at the isosbestic excitation wavelength. After addition of 10 μM TCS to perfusion buffer, ECCE was induced by high-frequency electrical stimuli using two platinum electrodes fixed to the well and Ca^{2+} entry was measured by the rate of quench of Fura-2 fluorescence. Ca^{2+}-mode measurement of ECCE required pretreatment of myotubes with 500 μM ryanodine for 30 min before exposure to TCS. After introduction of 10 μM TCS to buffer, ECCE was induced by electrical stimuli and Ca^{2+} was assessed as the rise in Fluo-4 fluorescence.

Measurement of Skeletal L-Type Ca^{2+} Current. Pipettes were fabricated from borosilicate glass and had resistances of ~2.0 MΩ when filled with internal solution, which consisted of: Cs-aspartate 140 mM, Cs_2-EGTA 10 mM, $MgCl_2$ 5 mM, and Hepes 10 mM, pH 7.4. The external solution contained: tetraethylammonium-Cl 145 mM, $CaCl_2$ 10 mM, tetrodotoxin 0.002 mM, and Hepes 10 mM, pH 7.4. Electronic compensation was used to reduce the effective series resistance (usually to < 1 MΩ) and the time constant for charging the linear cell capacitance (usually to

< 0.5 ms). L-type currents were corrected for linear components of leak and capacitive current by digital scaling and subtraction of the average of 11, 30-mV hyperpolarizing pulses from a holding potential of −80 mV. Filtering was at 2 kHz (eight-pole Bessel filter; Frequency Devices) and digitization was at 10 kHz (L-type currents). Voltage-clamp command pulses were exponentially rounded with a time constant of 50–500 μs and a 1-s prepulse to −20 mV followed by a 25-ms repolarization to −50 mV was administered before the test pulse to inactivate endogenous Ca_v3 and Na_v channels. Cell capacitance was determined by integration of a transient from −80 mV to −70 mV using Clampex 8.0 (Molecular Devices) and was used to normalize current amplitudes (pA/pF). L-type Ca^{2+} currents were measured before and 15–20 min after perfusion of TCS (10 μM) to myotubes. All electrophysiological experiments were performed at room temperature (~25 °C).

Preparations of Membrane Fractions from Mouse Skeletal Muscle. Sarcoplasmic reticulum (SR) microsomes were isolated from mouse skeletal muscle tissue as described in ref. 15. Briefly, skeletal muscles from wild-type mice were homogenized in ice-cold buffer containing 200 mM sucrose, 5 mM imidazole, 0.01 mM phenylmethylsulfonyl fluoride, and 5 μg/mL leupeptin, pH 7.4. Homogenates were differentially centrifuged at 10,000 × *g* (20 min) and 110,000 × *g* (60 min). Pellets were resuspended in 200 mM sucrose and 10 mM Hepes, pH 7.4, and flash frozen and stored at −80 °C.

Radioligand Binding Assay. Radioligand binding assays with [^{3}H]ryanodine and [^{3}H]PN200 were performed as previously described (15, 17). Specific radioligand binding was assessed for 0–20 μM TCS. [^{3}H]ryanodine binding assays were carried out in optimal Ca^{2+} (50 μM) with 2 nM radioligand, and [^{3}H]PN200 binding was assessed with both 1 and 10 nM radioligand. Each experiment was performed in triplicate and on two independent skeletal muscle preparations. Nonlinear curve fitting was performed using Prism (GraphPad Software).

1. Pacher P, Nagayama T, Mukhopadhyay P, Bátkai S, Kass DA (2008) Measurement of cardiac function using pressure-volume conductance catheter technique in mice and rats. *Nat Protoc* 3:1422–1434.
2. Schebb NH, et al. (2011) Investigation of human exposure to triclocarban after showering and preliminary evaluation of its biological effects. *Environ Sci Technol* 45: 3109–3115.
3. USEPA (2002) *Short-Term Methods for Estimating the Chronic Toxicity of Effluents and Receiving Waters to Freshwater Organisms* (US Environmental Protection Agency, Washington, DC).
4. USEPA (2002) *Methods for Measuring the Acute Toxicity of Effluents and Receiving Waters to Freshwater Organisms* (US Environmental Protection Agency, Washington, DC).
5. Heath AG, Cech JJ, Jr., Zinkl JG, Steele MD (1993) Sublethal effects of three pesticides on Japanese medaka. *Arch Environ Contam Toxicol* 25:485–491.
6. Beggel S, Werner I, Connon RE, Geist JP (2010) Sublethal toxicity of commercial insecticide formulations and their active ingredients to larval fathead minnow (*Pimephales promelas*). *Sci Total Environ* 408:3169–3175.
7. Li N, et al. (2009) Ablation of a Ca2+-activated K+ channel (SK2 channel) results in action potential prolongation in atrial myocytes and atrial fibrillation. *J Physiol* 587: 1087–1100.
8. Lu L, et al. (2007) Molecular coupling of a Ca2+-activated K+ channel to L-type Ca2+ channels via alpha-actinin2. *Circ Res* 100:112–120.
9. Babu GJ, et al. (2007) Ablation of sarcolipin enhances sarcoplasmic reticulum calcium transport and atrial contractility. *Proc Natl Acad Sci USA* 104:17867–17872.
10. Xu Y, et al. (2005) The effects of intracellular Ca2+ on cardiac K+ channel expression and activity: Novel insights from genetically altered mice. *J Physiol* 562: 745–758.
11. Hamill OP, Marty A, Neher E, Sakmann B, Sigworth FJ (1981) Improved patch-clamp techniques for high-resolution current recording from cells and cell-free membrane patches. *Pflugers Arch* 391(2):85–100.
12. Zhang Z, et al. (2002) Functional Roles of $Ca_{(v)}1.3$ ($\alpha_{(1D)}$) calcium channel in sinoatrial nodes: Insight gained using gene-targeted null mutant mice. *Circ Res* 90:981–987.
13. Cherednichenko G, et al. (2004) Conformational activation of Ca2+ entry by depolarization of skeletal myotubes. *Proc Natl Acad Sci USA* 101:15793–15798.
14. Brown LD, Rodney GG, Hernández-Ochoa E, Ward CW, Schneider MF (2007) Ca2+ sparks and T tubule reorganization in dedifferentiating adult mouse skeletal muscle fibers. *Am J Physiol Cell Physiol* 292:C1156–C1166.
15. Feng W, et al. (2011) Functional and biochemical properties of ryanodine receptor type 1 channels from heterozygous R163C malignant hyperthermia-susceptible mice. *Mol Pharmacol* 79:420–431.
16. Clementi E, et al. (1992) Receptor-activated Ca2+ influx. Two independently regulated mechanisms of influx stimulation coexist in neurosecretory PC12 cells. *J Biol Chem* 267:2164–2172.
17. Buck ED, Nguyen HT, Pessah IN, Allen PD (1997) Dyspedic mouse skeletal muscle expresses major elements of the triadic junction but lacks detectable ryanodine receptor protein and function. *J Biol Chem* 272:7360–7367.

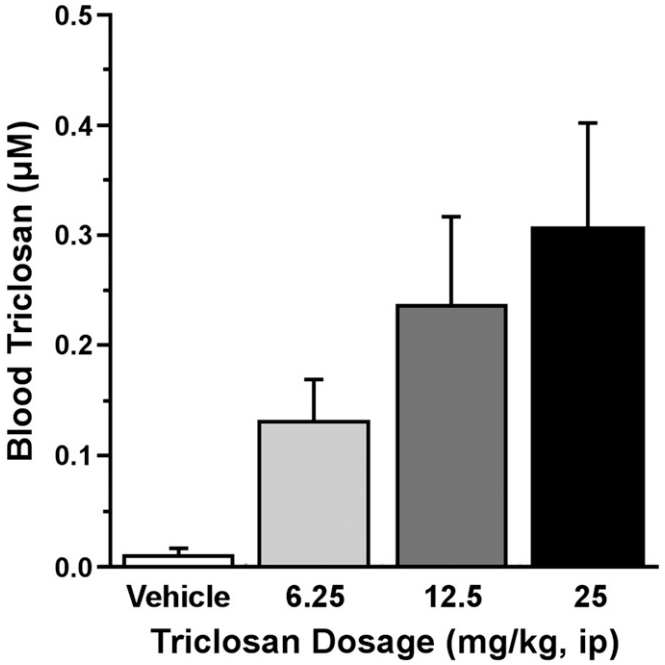

Fig. S1. TCS plasma levels following intraperitoneal administration to mice. Mice (vehicle: $n = 3$; TCS: $n = 6–9$) were exposed to 0–25 mg/kg TCS in DMSO via intraperitoneal injection. After 15 min, blood was collected and plasma TCS levels were determined by LC-ESI-MS. Error bars represent SEM.

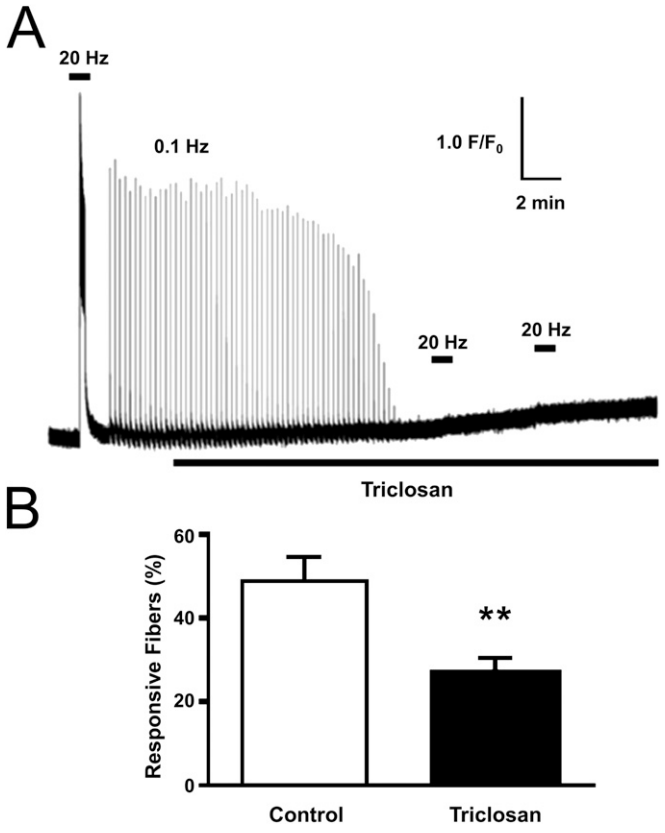

Fig. S2. TCS impairs ECC in adult mouse FDB fibers. (*A*) Adult FDB fibers were stimulated by electrical field at 20 Hz or 0.1 Hz. Perfusion of 10 μM TCS lead to a decrease in calcium transient amplitude and the eventual complete loss of EC coupling. No appreciable increase in resting Ca^{2+} levels was observed. (*B*) Adult FDB fibers were incubated with control ($n = 1,965$) or 0.5 μM TCS ($n = 2,239$) in serum-free medium for 24 h at 37 °C. The 0.5 μM TCS significantly reduced the number of adult FDB fibers with ECC by 44.7 ± 8.6%. Error bars represent SEM. $^{**}P < 0.01$, *t* test.

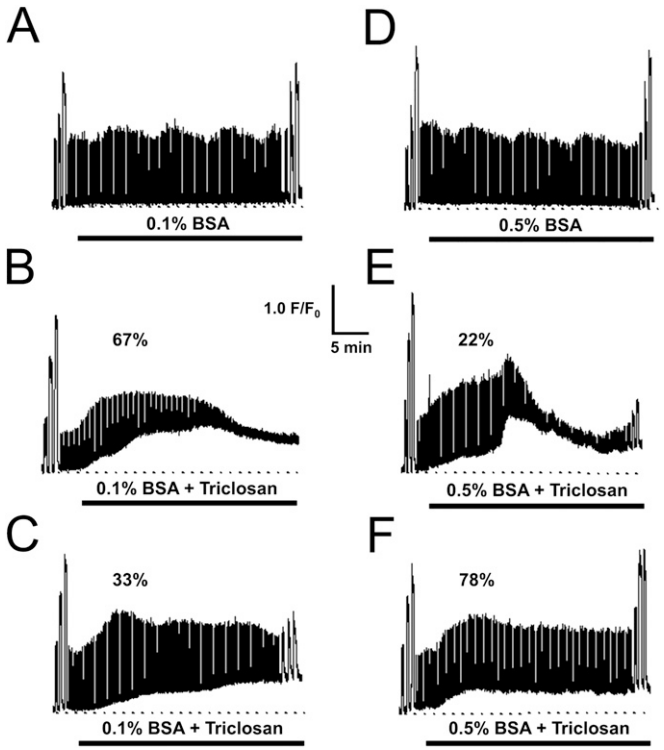

Fig. S3. Serum albumin mitigates—but does not completely eliminate—the effects of TCS on myotubes. Skeletal myotubes were perfused with 0 or 10 μM TCS in buffer with either 0.1% BSA (*A*–*C*) or 0.5% BSA (*D*–*F*). Without TCS, EC coupling was well-maintained over time in the presence of BSA (*A* and *D*). With 0.1% BSA, ECC failure occurred in 67% of the cells (*B*); the remaining cells retained partial ECC (*C*). The 0.5% BSA preserved ECC in 78% of the cells (*F*), yet several cells still exhibited severely reduced or complete loss of ECC (*E*). Serum albumin failed to prevent an increase in resting Ca^{2+} levels regardless of concentration (*B*, *C*, *E*, and *F*).

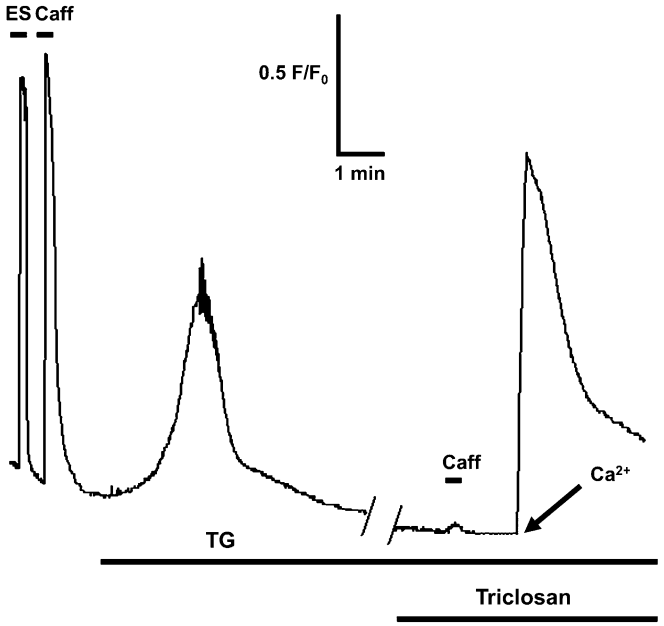

Fig. S4. SOCE is not affected by TCS. Skeletal myotubes were treated with 200 nM thapsigargan (TG) in Ca^{2+}-free buffer to inhibit activity of the sarcoplasmic/endoplasmic reticulum Ca^{2+} ATPase (SERCA). This induced a mobilization of Ca^{2+} and a complete depletion of SR Ca^{2+} stores, as evidenced by a lack of response to caffeine (Caff). Note that after store depletion, 10 μM TCS was unable to elicit an increase in resting Ca^{2+} level. Reintroduction of extracellular Ca^{2+} in the presence of TCS initiated a massive Ca^{2+} influx normally seen in naive cells.